Palaeogeography, Palaeoclimatology, Palaeoecology 699 (2026) 114032

Contents lists available at ScienceDirect

Palaeogeography, Palaeoclimatology, Palaeoecology

journal homepage: www.elsevier.com/locate/palaeo

Middle-late Devonian warming and land plant evolution drive changes in silicate weathering: A new $^{87}Sr/^{86}Sr$ conodont record paired with $\delta^{18}O$

Teresa D. Avila [a], Matthew R. Saltzman [a,*], Michael M. Joachimski [b], Elizabeth M. Griffith [a], Benjamin J.W. Mills [c]

[a] School of Earth Sciences, Ohio State University, Columbus, OH, USA
[b] GeoZentrum Nordbayern, Friedrich-Alexander University Erlangen-Nürnberg (FAU), Erlangen, Germany
[c] School of Earth and Environment, University of Leeds, Leeds, UK

A R T I C L E I N F O

Editor: Thomas Steuber

Keywords:
Carbon cycle
Frasnian
Givetian
Climate model
First trees

A B S T R A C T

The Devonian Period (419 to 359 Ma) is marked by a shift from cooling in the Early Devonian to warming in the Middle-Late Devonian. Previous studies have hypothesized that an increase in metamorphic degassing during the Acadian Orogeny caused the late Givetian warming. Alternatively, a reduction in physical erosion leading to reduced silicate weathering could have increased pCO_2 and contributed to warming. Previous studies show that the $^{87}Sr/^{86}Sr$ curve of the Middle Devonian (late Givetian) increases (i.e., more granitic) around the same time as warming based on $\delta^{18}O$ using brachiopod calcite. We present new Middle to Late Devonian $^{87}Sr/^{86}Sr$ and $\delta^{18}O$ data from conodont apatite and confirm this link between warming and rising $^{87}Sr/^{86}Sr$ using paired analyses from a single measured section whereas previous studies relied on compiling data from different sections that did not individually capture the baseline values and subsequent shifts in proxies. We integrate these datasets into the SCION climate-biogeochemical model and determine that the hypothesized magnitude of metamorphic degassing could neither reproduce the seawater $^{87}Sr/^{86}Sr$ ratio nor explain the extent of low-latitude warming ($\delta^{18}O$) observed in the geologic record. An alternative warming mechanism is rising atmospheric pCO_2 due to reduced physical erosion and silicate weathering related to land plant colonization. Regional uplift of high $^{87}Sr/^{86}Sr$ rocks in the Acadian orogeny may have driven the increasing seawater $^{87}Sr/^{86}Sr$ ratio.

1. Introduction

The Devonian Period (419 to 359 Ma) represents a dynamic time in Earth's climate history marked by large swings in temperature (Joachimski et al., 2009; Chen et al., 2021; Grossman and Joachimski, 2022). Major biological crises took place during the Middle to Late Devonian (Bambach, 2006; Kabanov et al., 2023), and vascular plants were established by the late Middle Devonian, likely contributing to drawdown of atmospheric CO_2 (e.g., Le Hir et al., 2011) and an increase in O_2 (e.g., Dahl and Arens, 2020; Elrick et al., 2022). A major warming episode in the late Givetian Stage (van Geldern et al., 2006; Joachimski et al., 2009) across the Middle-Late Devonian transition is associated with coral-stromatoporoid reef expansion (Qie et al., 2019; Huang et al., 2025). The late Givetian is also marked by a significant increase in seawater strontium isotopes ($^{87}Sr/^{86}Sr$) that may be linked to changes in silicate rock weathering (van Geldern et al., 2006), potentially providing insights into Devonian climate evolution.

The late Givetian $^{87}Sr/^{86}Sr$ increase (van Geldern et al., 2006) encompasses an 8 to 10 °C warming based on $d^{18}O$ (Chen et al., 2021; Joachimski et al., 2009; Stewart and Ague, 2018). The driver of late Givetian warming may have been a pulse of metamorphic degassing during the Acadian Orogeny (Stewart and Ague, 2018; Chen et al., 2021) or reduced silicate weathering as vascular plant colonization lowered physical erosion (Maffre et al., 2022). The warming was proposed as the driver for the $^{87}Sr/^{86}Sr$ increase in the late Givetian, through enhanced weathering of radiogenic Gondwanan continental crust (van Geldern et al., 2006). However, the effects of land plant colonization on erosion require a spatially resolved perspective on where the uplift of mountain belts occurred and where weathering was most intense.

Although van Geldern et al. (2006) first linked the late Givetian $^{87}Sr/^{86}Sr$ increase with a $d^{18}O$ decrease (warming), the inflections in the isotope curves that suggest a coincident timing are based on six brachiopod samples on which paired Sr and O were conducted (four brachiopod samples from one quarry in Iowa, one from a core in Iowa,

* Corresponding author.
E-mail address: saltzman.11@osu.edu (M.R. Saltzman).

https://doi.org/10.1016/j.palaeo.2026.114032
Received 8 April 2026; Received in revised form 28 June 2026; Accepted 29 June 2026
Available online 30 June 2026

and another from an outcrop in Spain). However, none of the three localities utilized provides a continuous record of paired $^{87}Sr/^{86}Sr$ and $d^{18}O$ values through the inflection interval (van Geldern et al., 2006), raising important questions about the timing. While the $^{87}Sr/^{86}Sr$ record is generally considered to be a global signal because of the long residence time of Sr in the oceans (McArthur et al., 2020), the $d^{18}O$ record in a given region is known to vary based on the temperature and salinity (Joachimski et al., 2009; Chen et al., 2021). This is the case in the late Givetian to Frasnian (Middle to Late Devonian) transition where the timing and magnitude of paleotemperature changes in intensively sampled North American (Iowa, USA), European (France) and South China sections differ by millions of years (Chen et al., 2021).

This paper addresses questions about the timing of changes in weathering and paleotemperature proxies by pairing $^{87}Sr/^{86}Sr$ and $d^{18}O$ in a European section which offers the most complete and coherent record of the late Givetian warming. We present new Middle to Late Devonian $^{87}Sr/^{86}Sr$ data from conodont apatite from the Pic de Bissous section in the Montagne Noire, France. Our $^{87}Sr/^{86}Sr$ data are paired with published oxygen isotope data from the same conodont samples at Pic de Bissous (Joachimski et al., 2009).

2. Background

2.1. $^{87}Sr/^{86}Sr$ as a geochemical proxy for silicate weathering

Seawater $^{87}Sr/^{86}Sr$ serves as a proxy for global silicate weathering patterns, primarily reflecting changes in the dominant lithology undergoing weathering (Peucker-Ehrenbrink and Fiske, 2019). Strontium

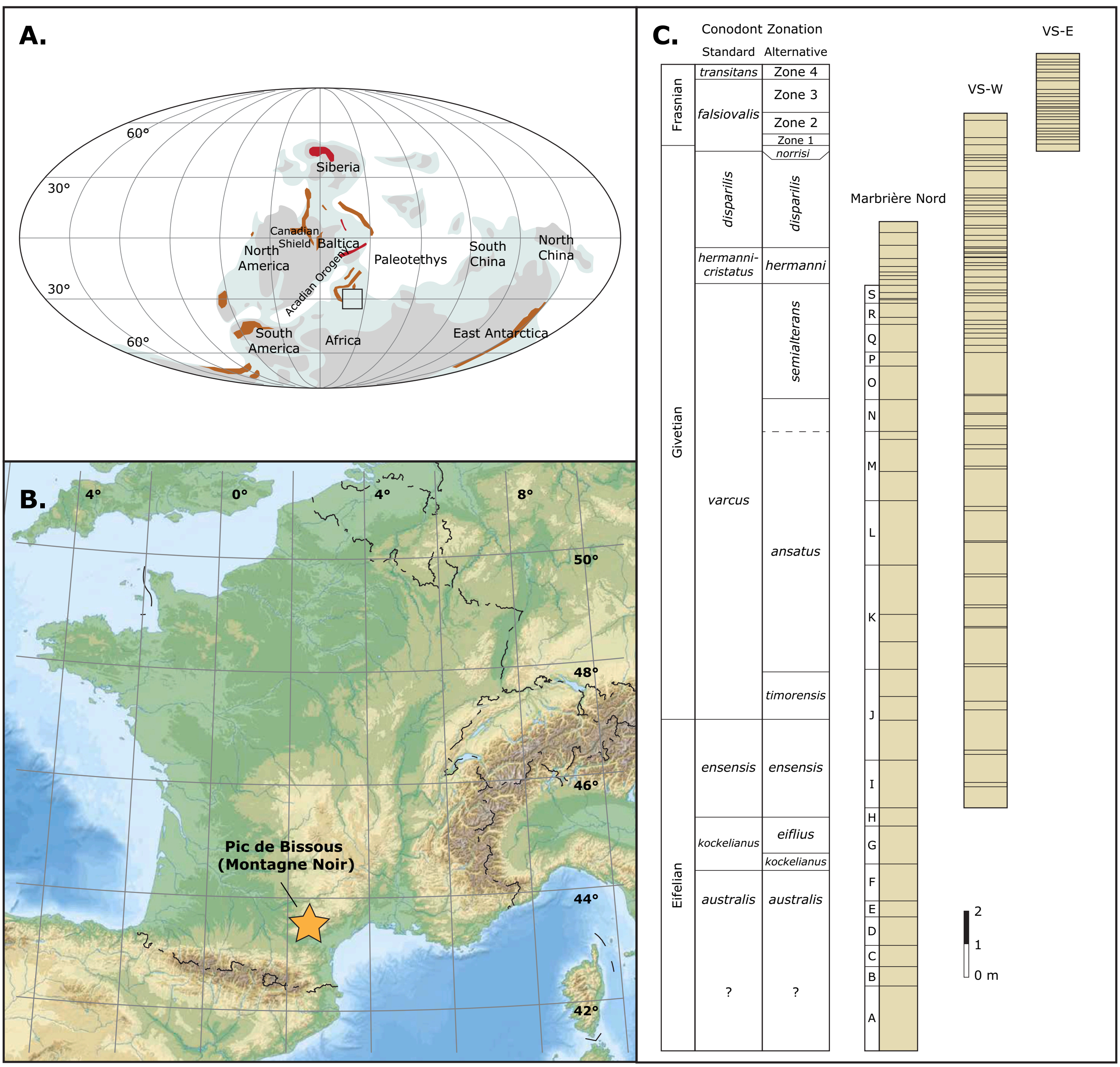

Fig. 1. A. Paleogeographic reconstruction for the Middle to Late Devonian following Joachimski et al. (2009) and Chen et al. (2021). Gray = land; blue = continental shelf; white = open ocean; brown = collision belts; red = LIPs. B. Map of modern-day France (taken from Wikimedia Commons) with location of Pic de Bissous and the Montagne Noire indicated by star. C. The Pic de Bissous sequence shown across three exposed sections: Marbrière Nord, VS-W, and VS-E. All sections are composed of carbonates (in tan). Meters and conodont zonation taken from Feist (2002). (For interpretation of the references to colour in this figure legend, the reader is referred to the web version of this article.)

fluxes to the ocean derive primarily from weathering of continental rocks transported to the oceans in rivers and groundwater as well as hydrothermal activity. The hydrothermal Sr flux typically has an $^{87}Sr/^{86}Sr$ value of ~0.7084 (Elderfield and Schultz, 1996) and tends to drive the global seawater $^{87}Sr/^{86}Sr$ curve toward lower, less radiogenic values. The $^{87}Sr/^{86}Sr$ ratio of the riverine Sr flux (encompassing both surficial runoff and groundwater) can be influenced by granitic (Elderfield and Schultz, 1996; Basu et al., 2001) or basaltic lithologies (Swanson-Hysell and Macdonald, 2017; Macdonald et al., 2019). The average $^{87}Sr/^{86}Sr$ value for the riverine Sr flux is ~0.7119 (Elderfield and Schultz, 1996) and tends to drive the global seawater $^{87}Sr/^{86}Sr$ curve toward higher, more radiogenic values.

2.2. Study site

The Montagne Noire is located in central southern France. The Pic de Bissous sequence comprises three exposed sections spanning the Eifelian to early Frasnian: the Marbrière Nord, VS-W, and VS-E (Feist, 1985, 2002) (Fig. 1). The sequence is composed of carbonates, — including well-oxygenated mud- and wackestones (Feist, 1985, 2002; Buggisch and Joachimski, 2006). The section is interpreted to represent a carbonate ramp depositional environment in the Paleotethys, south of Laurussia (i.e., the combined continental mass of Laurentia and Baltica) and north of Gondwana (Fig. 1).

3. Method

3.1. Sample acquisition

Conodont apatite samples analyzed here for $^{87}Sr/^{86}Sr$ are the same samples used in Joachimski et al. (2009). The Pic de Bissous conodont elements are a range of morphologies (i.e., cone, blade, platform, and fragments) with conodont alteration index (CAI) ranging from 3 to 5 (Avila et al., 2025; Epstein et al., 1977).

3.2. Sample preparation

Seventeen conodont apatite samples were analyzed for $^{87}Sr/^{86}Sr$. Depending on sample availability, approximately 1.8 mg of conodont elements were selected from each sample. The elements were then sonicated three times in Milli-Q deionized water to remove debris. The elements were leached in 0.5 mL of 5% acetic acid (CH_3COOH) for ~18 h, following the methods of Avila et al. (2022, 2025). For each sample the leachate was saved. For three samples (MN 138, 135, and 98) the amount of Sr in the leachate was sufficient for $^{87}Sr/^{86}Sr$ analysis. This enabled us to compare the $^{87}Sr/^{86}Sr$ in the leachate with that of the conodont sample (Fig. 2) and to establish that leaching had removed a statistically significant amount of radiogenic Sr. For more details on leaching, see Appendix A of the Supplementary Material and Tables S2, S3.

After leaching, conodont elements were dissolved in 6 N HCl overnight, and the resulting solution was dried down on a hot plate. The samples were brought back up in 2% HNO_3 and an aliquot was removed for Sr concentration analysis on an Inductively Coupled Plasma Mass Spectrometer (ICP-MS) in the Trace Element Research Laboratory at Ohio State University. Separation of the samples' Sr fraction was done using 6 mL glass columns filled with BioRad AG 50 W-X8 resin (Foland and Allen, 1991) followed by a second set of columns using Eichrom Industries Sr-Spec resin in 125 μL Teflon microcolumns (Scher et al., 2014).

3.3. $^{87}Sr/^{86}Sr$ analysis

$^{87}Sr/^{86}Sr$ analyses were conducted on a Thermal Ionization Mass Spectrometer (TIMS) in the Thermal Ionization Mass Spectrometry Laboratory at Ohio State University. We loaded purified Sr fractions

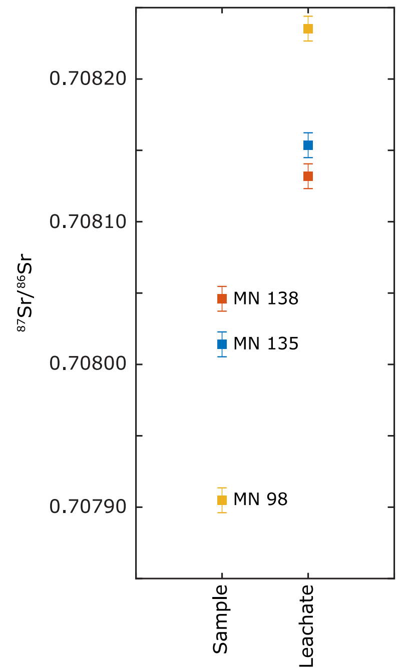

Fig. 2. Comparison of $^{87}Sr/^{86}Sr$ values of samples (MN 138, 135, and 98) and their respective leachates. Error bars represent external analytical uncertainty (9×10^{-6}).

onto a rhenium ribbon with a Ta_2O_5 activator using a single-filament setup. SRM 987 was used as a standard, with an average measured value of 0.710253 (2SD = 2.2×10^{-5}; $n = 114$; analyzed from 1/31/18 to 1/30/20) to enable comparison with prior results and to eliminate any drift. Potential ^{87}Rb contamination was accounted for by measuring ^{85}Rb and using the assumed $^{87}Rb/^{85}Rb$ value 0.386000 (Steiger and Jäger, 1977). We also accounted for instrument mass fractionation by normalizing $^{87}Sr/^{86}Sr$ values to an assumed $^{88}Sr/^{86}Sr$ ratio of 8.375 (Steiger and Jäger, 1977).

Out of 17 conodont apatite samples, 16 were successfully analyzed for $^{87}Sr/^{86}Sr$ (Table S1 in Supplementary Material; Fig. 3). The uncertainty associated with each individual $^{87}Sr/^{86}Sr$ analysis (i.e., internal analytical uncertainty) is defined as the absolute standard error of 200 measurements per sample. On average, this uncertainty is 3×10^{-6} ($n = 16$). The uncertainty associated with replicate sample analyses (i.e., external analytical uncertainty) is defined as two standard deviations of repeated measurements of standard SRM 987; this value is 9×10^{-6} (n = 114). The average Sr concentration for the conodont apatite is 2583 ppm (2SD = 1263 ppm; $n = 17$).

3.4. Conodont $\delta^{18}O$ values

The original $\delta^{18}O$ analyses conducted by Joachimski et al. (2009) were calibrated to a value of 22.4‰ for the NBS 120c standard. Since the accepted value for NBS 120c is now 21.7‰ (e.g., Chenery et al., 2010), we subtracted 0.7‰ from the originally reported $\delta^{18}O$ values.

4. Results

$^{87}Sr/^{86}Sr$ values from the Eifelian to late Givetian *P. costatus* to *O. semialterans* conodont zones form a baseline ranging between ~0.7079 and 0.7080 (Fig. 3). Across the late Givetian *P. ectypus, S. hermanni*, and *O. semialterans* zones (~380 Ma), $^{87}Sr/^{86}Sr$ shifts toward values ranging between ~0.7080 and 0.7081. The six uppermost samples (MN 127 to MN 140) demonstrate a consistent increase from 0.707919 to 0.708070, i.e., an increase of 0.000151 over the course of ca. 2 My (Fig. 3).

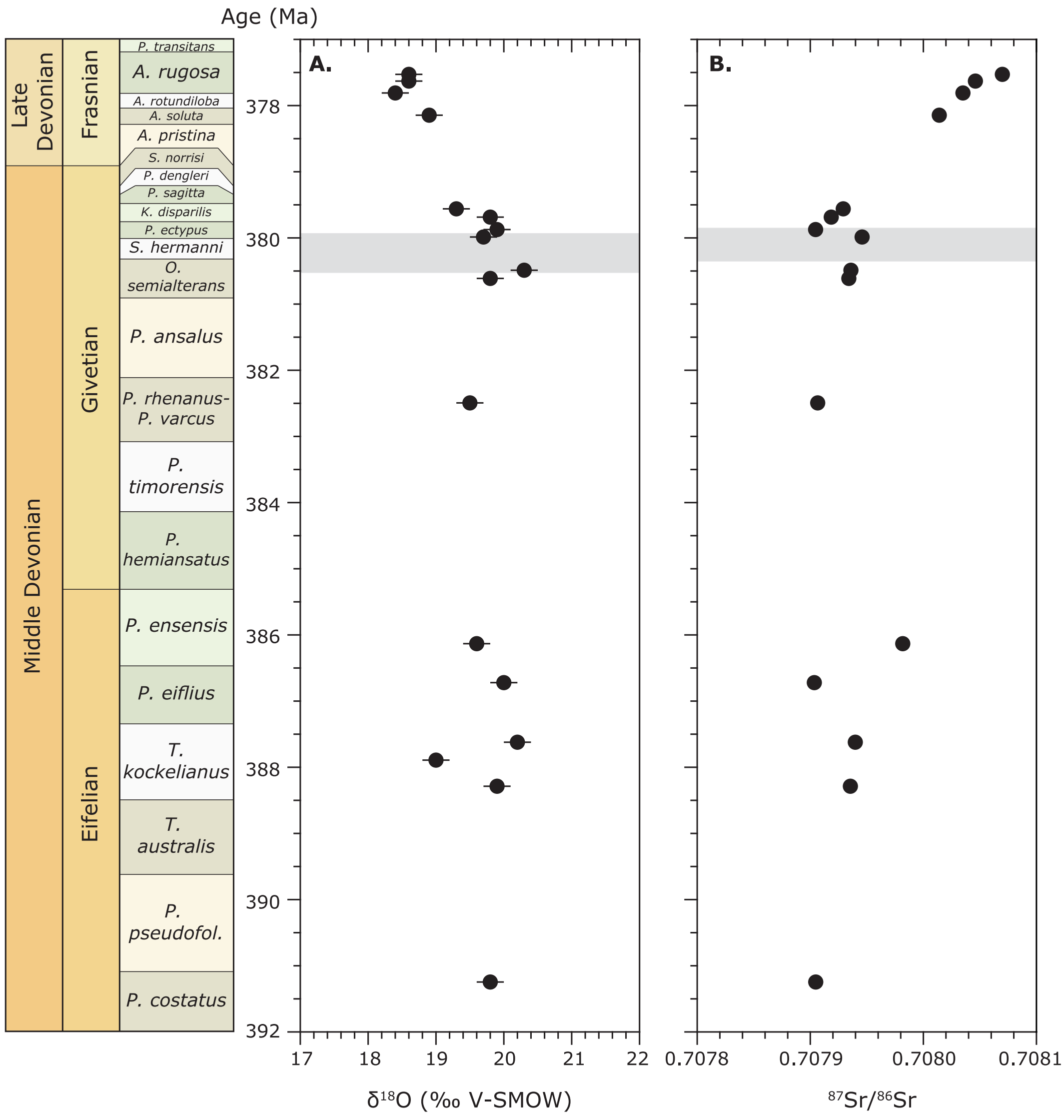

Fig. 3. A. Pic de Bissous $\delta^{18}O$ data from Joachimski et al. (2009) with original values corrected by −0.7‰ for updated value of standard NBS120c of 21.7‰ VSMOW. Error bars give analytical reproducibility (1 standard deviation). B. $^{87}Sr/^{86}Sr$ data from this study. Error is defined as external analytical error; error bars are smaller than data points. Gray bar highlights general period of time in which both Sr and O isotopes are changing. Period ages and conodont zonation from GTS 2020 in Becker et al. (2020), which are converted from original conodont zonation of Joachimski et al. (2009).

5. Discussion

5.1. Diagenesis and conodont apatite $^{87}Sr/^{86}Sr$

Diagenesis via thermal alteration, recrystallization, or exchange with porewaters can alter conodont apatite $^{87}Sr/^{86}Sr$ (Avila et al., 2025; Conwell et al., 2026; Holmden, 1996; John et al., 2008; Saltzman et al., 2014), potentially shifting it to higher (more radiogenic) values (e.g., Epstein et al., 1977; Martin and Scher, 2004; Dudás et al., 2017). Thermal alteration typically occurs when conodont elements are exposed to regional, contact, or hydrothermal metamorphism (i.e., metamorphism specifically resulting from interaction with high-temperature, chemically active fluids). With increasing temperature, the colour of conodont elements turns from pale yellow to black due to the maturation of enclosed organic matter as measured by the Colour Alteration Index (CAI) (Epstein et al., 1977; Zhang et al., 2026). Despite differences in CAI, $^{87}Sr/^{86}Sr$ data derived from conodont apatite shows comparable trends to brachiopod calcite as long as the enclosing rock type is carbonate and not shale (Conwell et al., 2026; McArthur et al., 2020; Saltzman et al., 2014). In this study, conodont samples have a CAI ranging from 3 to 5, suggesting alteration temperatures ranging as high as 200 to 300 °C (Epstein et al., 1977). The compiled $^{87}Sr/^{86}Sr$ curve is ~0.00011 higher compared to the Eifelian to Frasnian curve derived from brachiopod calcite (van Geldern et al., 2006) (Fig. 4). Throughout the ~0.0001 late Givetian increase in $^{87}Sr/^{86}Sr$, from about 0.70782 to 0.70792 in brachiopod calcite and from 0.70793 to 0.70803 in conodont apatite, the magnitude of the offset maintains a similar range that averages ~0.00011 ± 0.00003 (offsets for individual samples compared by closest age tie point range from as low as 0.000064 to as high as 0.000165) (Table S1 and Fig. 4).

Our results showing slightly higher $^{87}Sr/^{86}Sr$ (0.0001) in higher CAI conodonts can be compared with similar efforts to assess diagenesis in $\delta^{18}O$ based on CAI. Joachimski et al. (2009) observed that trends in $\delta^{18}O$ of Devonian conodonts were comparable among conodonts with CAI ranging from 1 to 5, despite the fact that recrystallization in conodont apatite begins at CAI 5 or higher (i.e., low grade metamorphism). Therefore, the Pic de Bissous $^{87}Sr/^{86}Sr$ data appear to be useful in this study because the focus is on relative changes in the seawater $^{87}Sr/^{86}Sr$ value rather than the absolute value that is more important for correlation studies.

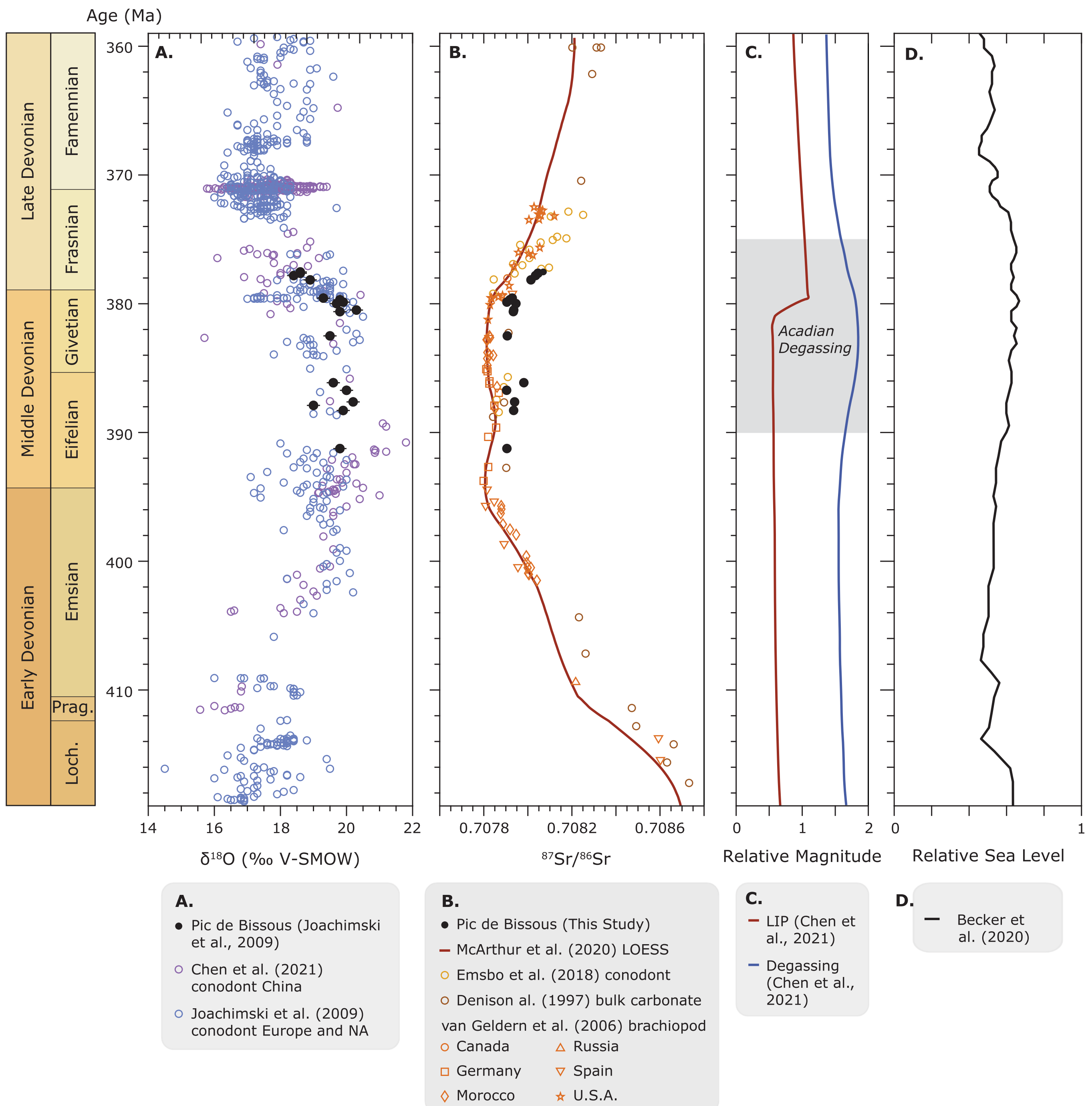

Fig. 4. Comparison of $\delta^{18}O$, $^{87}Sr/^{86}Sr$, degassing rate, and eustatic sea level. A. Conodont $\delta^{18}O$ data from Joachimski et al. (2009) and Chen et al. (2021). B. $^{87}Sr/^{86}Sr$ data from this study, Emsbo et al. (2018), van Geldern et al. (2006), Denison et al. (1997), and LOESS curve from McArthur et al. (2020). van Geldern et al. (2006) data is differentiated by country. Note that through the ~0.0001 late Givetian increase in $^{87}Sr/^{86}Sr$, which increases from ~0.70782 to 0.70792 in brachiopod calcite, the magnitude of the offset in conodont apatite maintains a similar range that averages ~0.00011 ± 0.00003. C. Unitless relative magnitude of degassing rate (blue) and LIP area (red) from Chen et al. (2021). Gray box demonstrates estimated interval of Acadian metamorphic degassing. D. Eustatic sea level curve (unitless) from Becker et al. (2020). (For interpretation of the references to colour in this figure legend, the reader is referred to the web version of this article.)

5.2. Late Givetian inflections in $^{87}Sr/^{86}Sr$ and $\delta^{18}O$

Our paired $^{87}Sr/^{86}Sr$ and $\delta^{18}O$ study of conodont apatite in the Pic de Bissous section complements previous Devonian-age $^{87}Sr/^{86}Sr$ and $\delta^{18}O$ studies that compiled data from around the world (van Geldern et al., 2006; Joachimski et al., 2009; Chen et al., 2021) using brachiopod calcite and conodont apatite. From 392 to 377 Ma, the van Geldern et al. (2006) $^{87}Sr/^{86}Sr$ dataset is based on brachiopod samples from 21 sections across Canada, Germany, Morocco, Russia, Spain, and U.S.A. (Fig. 4). In terms of $\delta^{18}O$, the Joachimski et al. (2009) conodont data set is compiled from 8 sections across Czech Republic, France, Germany, and U.S.A., and the Chen et al. (2021) dataset is compiled from 5 sections across China. The fact that these studies derive from multiple locations means the observed trends are likely global, with the larger spread in $\delta^{18}O$ likely resulting from regional differences in seawater temperature and factors influencing $\delta^{18}O$ of sea water. However, comparing the shifts in $^{87}Sr/^{86}Sr$ and $\delta^{18}O$ is difficult due to the uncertainty inherent in biostratigraphically correlating sections from multiple regions. Furthermore, whereas brachiopod calcite analyses are conducted on single shells, in order to obtain enough conodont apatite for $\delta^{18}O$ the samples must be combined through several dissolved rock layers that are time averaged. This further complicates assessment of coincidence in timing and causal connections between $^{87}Sr/^{86}Sr$ and $\delta^{18}O$ when comparing different compilations.

The study of van Geldern et al. (2006) was the first to recognize that the late Givetian $^{87}Sr/^{86}Sr$ increase coincided with a $d^{18}O$ decrease (warming). In that study, paired $^{87}Sr/^{86}Sr$ and $d^{18}O$ were measured on six individual brachiopod samples, including four from the Buffalo Quarry in Iowa, one from the IPSCO core in Iowa, and one from the Cantabrian Mountains in Spain. Because the three localities did not provide a continuous record through the inflections in $^{87}Sr/^{86}Sr$ and $d^{18}O$ through the late Givetian (van Geldern et al., 2006), this left open questions about timing. While $^{87}Sr/^{86}Sr$ is considered to be a global signal because of the long residence time of Sr in the oceans (McArthur et al., 2020), $d^{18}O$ varies between regions with temperature and salinity (Joachimski et al., 2009; Chen et al., 2021). In the late Givetian to Frasnian (Middle to Late Devonian) transition, the timing and magnitude of $d^{18}O$-derived paleotemperature changes in intensively sampled North American (Iowa, USA), European (France) and South China sections differ by millions of years (Chen et al., 2021). Our study shows that in the Pic de Bissous section, the $^{87}Sr/^{86}Sr$ seawater curve shifts beginning in the late Givetian and correlates with the $\delta^{18}O$ shift from ~19.8 to ~18.6‰ V-SMOW (Joachimski et al., 2009) (Fig. 4). In the following sections, we first address potential causes of the increase in $^{87}Sr/^{86}Sr$ using isotope mass balance modeling, and then examine potential links between $^{87}Sr/^{86}Sr$ and $\delta^{18}O$ using SCION, a global biogeochemical model that incorporates both climate and continental weathering on a spatial scale.

5.3. Potential drivers of increasing late Givetian seawater $^{87}Sr/^{86}Sr$

The factors needed to drive an increase in seawater $^{87}Sr/^{86}Sr$ during the Givetian can be addressed using a deterministic (forward) Sr box model. The model operates by solving a set of Sr isotopic mass balance equations (Eq. 1 and 2) (e.g., Ingram et al., 1994):

$$\frac{dN}{dt} = J_{riv} + J_h - J_{carb} \tag{1}$$

$$N\frac{dR_{sw}}{dt} = J_{riv}(R_{riv} - R_{sw}) + J_h(R_h - R_{sw}) \tag{2}$$

where t is time; N is total moles of Sr in the ocean; J_{riv} and J_h are riverine and hydrothermal flux respectively; J_{carb} is the carbonate burial flux of Sr; R_{riv}, R_h, and R_{sw} are riverine, hydrothermal, and seawater $^{87}Sr/^{86}Sr$, respectively. Using this box model, the trend toward more radiogenic $^{87}Sr/^{86}Sr$ values could theoretically derive from: 1) a decrease in the hydrothermal Sr flux, 2) an increase in the hydrothermal $^{87}Sr/^{86}Sr$ ratio, 3) an increase in the riverine Sr flux, or 4) an increase in the riverine $^{87}Sr/^{86}Sr$ ratio. We consider how each of these factors were changing during the Middle to Late Devonian and model their potential impact on seawater $^{87}Sr/^{86}Sr$.

Changes in the hydrothermal flux have been modeled using inversion of eustatic sea level changes, using the assumption that long term ($> 10^6$ yrs) sea level in the absence of ice buildup has a linear relationship to the rate of seafloor production at mid-ocean ridges (e.g., Gaffin, 1987; Mills et al., 2017; Avila et al., 2022). Multiple studies have concluded that eustatic sea level was rising during the Middle to Late Devonian, resulting in the deposition of the Kaskaskia Sequence (e.g., Haq and Schutter, 2008; Qie et al., 2019; Becker et al., 2020). However, it should be noted that sea level changes related to seafloor production may be too slow to influence seawater $^{87}Sr/^{86}Sr$ on the timescale observed, and other potential drivers of sea level change include 2nd order glacio-eustasy (long period Milankovitch cycle) (Elrick, 2022; Elrick et al., 2009; Read et al., 2023). Therefore, we can consider both the modeled case here of sea level inversion and then consider an alternative in which tectono-eustasy is either not present in the Middle-Late Devonian study interval or too slow to affect our modeled seawater $^{87}Sr/^{86}Sr$.

In the case where seafloor spreading rates are changing, a higher spreading rate results in increased hydrothermal flow and a greater flux of basalt-derived Sr (e.g., Jones and Jenkyns, 2001; Coogan and Gillis, 2018). At the same time, increased seafloor production creates more young, warm, and buoyant mid-ocean ridge basalts (MORBs) that volumetrically replace seawater (e.g., Gaffin, 1987). Theoretically, an increase in seafloor production (if eustatic sea level was rising for this reason during the Middle to Late Devonian, which is not the only potential driver that also includes long term Milankovitch cycles; Elrick et al., 2009) will drive seawater $^{87}Sr/^{86}Sr$ to lower, less radiogenic values, which is not reflected in the data. A deterministic box model demonstrates that, all else held constant, a hydrothermal Sr flux following the eustatic sea level of Becker et al. (2020) does not recreate the seawater $^{87}Sr/^{86}Sr$ curve (Fig. S1 in Supplementary Materials).

Next, we consider whether the $^{87}Sr/^{86}Sr$ of the hydrothermal flux may have changed during the Middle Devonian. A shift in the relative concentrations of Ca, Mg, Sr, and SO_4 in seawater entering mid-ocean-ridge hydrothermal systems can affect the $^{87}Sr/^{86}Sr$ of the exiting hydrothermal fluid because seawater chemistry influences the relative proportions of seawater-derived Sr retained in solution versus basalt-derived Sr added during fluid–rock reaction (Antonelli et al., 2017). Antonelli et al. (2017) use data from ophiolites to provide the basis to calculate that hydrothermal $^{87}Sr/^{86}Sr$ increased during the Early Devonian, reached a peak, then decreased during the Middle and Late Devonian. The authors estimate the hydrothermal $^{87}Sr/^{86}Sr$ value to be ~0.7068 at 394 Ma, compared to the modern value of ~0.7033–0.7037 (e.g., Elderfield and Schultz, 1996; Jones and Jenkyns, 2001). In a second deterministic box model, we hold all other variables constant and use the change in the hydrothermal $^{87}Sr/^{86}Sr$ flux according to Antonelli et al. (2017). The modeled $^{87}Sr/^{86}Sr$ seawater curve decreases, opposite to our observations (Fig. S2 in Supplementary Materials). Therefore, riverine weathering likely drove $^{87}Sr/^{86}Sr$ up, and moreover, overrode the non-radiogenic influence of the hydrothermal flux. This is reasonable, as the riverine Sr flux is roughly twice the hydrothermal Sr flux (Elderfield and Schultz, 1996); however, this is not a unique interpretation and we consider other drivers below.

The impact of the riverine Sr flux may be significant and a major control over the rate of riverine weathering input is the amount of land exposed at lower latitudes (e.g., Marcilly et al., 2021). Land mass in the low-latitude belt (between ~10°N to 10°S) has an outsized impact on the Sr cycle and climate due to the relatively higher weathering rates (e.g., Macdonald et al., 2019). According to several paleogeographic models, the equatorial region during the Middle to Late Devonian was likely dominated by ocean; exposed land included portions of Laurussia (i.e., the combined continental mass of Laurentia and Baltica) and what is now China (e.g., Torsvik and Cocks, 2017; Golonka, 2020; Marcilly et al., 2021) (Fig. 1). Moreover, Marcilly et al. (2021) estimate that landmass in low latitudes rose by ~3% during this period. This appears to complement the ~5% decrease in exposed land at ±40–50°, as Laurussia shifted north, South China shifted south further into the low-latitude belt, and a northern peninsula of Gondwana shifted south and out of the low-latitude belt (Marcilly et al., 2021; Torsvik and Cocks, 2017). Once again, we use a deterministic Sr box model to hold all other factors static and assume that the 3% increase in low-latitude exposed land translates to a 3% increase in the riverine Sr flux. The result (Fig. S3 in Supplementary Figures) produces a modeled $^{87}Sr/^{86}Sr$ curve that increases but does so gradually and does not show the inflection at ca. 380 Ma. Therefore, increasingly low-latitude landmasses via plate motion may have contributed to increasing seawater $^{87}Sr/^{86}Sr$ but did not drive the 380 Ma inflection.

The increase in low-latitude land exposure likely also impacted the riverine flux's $^{87}Sr/^{86}Sr$ value. This is especially true for Laurussia, which experienced continental uplift during the Acadian Orogeny, part of the Ordovician to Devonian-age Appalachian-Caledonide-Variscan orogeny which encompassed the closing of the Iapetus and Rheic oceans that eventually formed Pangea (e.g., Murphy and Keppie, 2005; van Staal et al., 2009). In the literature, the Acadian typically refers to the Late Silurian to Early-Middle Devonian accretion of the Avalonia microcontinent to eastern Laurussia and closure of the Iapetus Ocean (e.g., Murphy and Keppie, 2005; van Staal et al., 2009). The result is an orogen that uplifted continental (i.e., granitic) material within subtropical latitudes, creating a weathering source of radiogenic Sr (e.g., Chen et al., 2021). Therefore, we propose that weathering of the Acadian Orogen likely drove seawater $^{87}Sr/^{86}Sr$ to a more radiogenic value. A final deterministic box model (Fig. 5) demonstrates that a 5×10^{-4} increase in riverine $^{87}Sr/^{86}Sr$ over the course of ca. 2–3 Ma can reproduce the proxy data. However, this increase in $^{87}Sr/^{86}Sr$ over 2–3 My is only constrained by creating a best-fit to our new data and is not a unique solution.

From these four deterministic box models, we conclude that changes in the hydrothermal Sr flux, hydrothermal $^{87}Sr/^{86}Sr$, and the riverine Sr flux were unlikely to have driven the seawater $^{87}Sr/^{86}Sr$ curve. This leaves changes in the riverine $^{87}Sr/^{86}Sr$ as the likely main driver. We now use SCION, a global biogeochemical model that incorporates both climate and continental weathering on a spatial scale, to determine whether an increase in riverine $^{87}Sr/^{86}Sr$ related to weathering of the Acadian Orogeny could have been driven by warming caused by a pulse of metamorphic degassing.

5.4. *Warming as a driver of late Givetian silicate weathering*

Overall, modeled atmospheric pCO_2 declined during the Middle to Late Devonian (e.g. Mills et al., 2017; Lenton et al., 2018), but an increase occurred based on a hypothesized metamorphic degassing event (Stewart and Ague, 2018; Chen et al., 2021). It is further hypothesized that the subsequent increase in LIP area mitigated the rise in CO_2 driven by this metamorphic degassing event (Racki, 2020). Chen et al. (2021) used the COPSE (Carbon-Oxygen-Phosphorus-Sulfur-Evolution) biogeochemical box model to investigate an increase in metamorphic degassing (Fig. 4) at ~390 Ma derived from water-bearing fluid infiltration of continental material during prograde metamorphism in the Acadian orogenic belt (Stewart and Ague, 2018). The process is estimated to have injected ~0.7 to 2.5×10^{19} mol CO_2 into the atmosphere (Stewart and Ague, 2018; Chen et al., 2021).

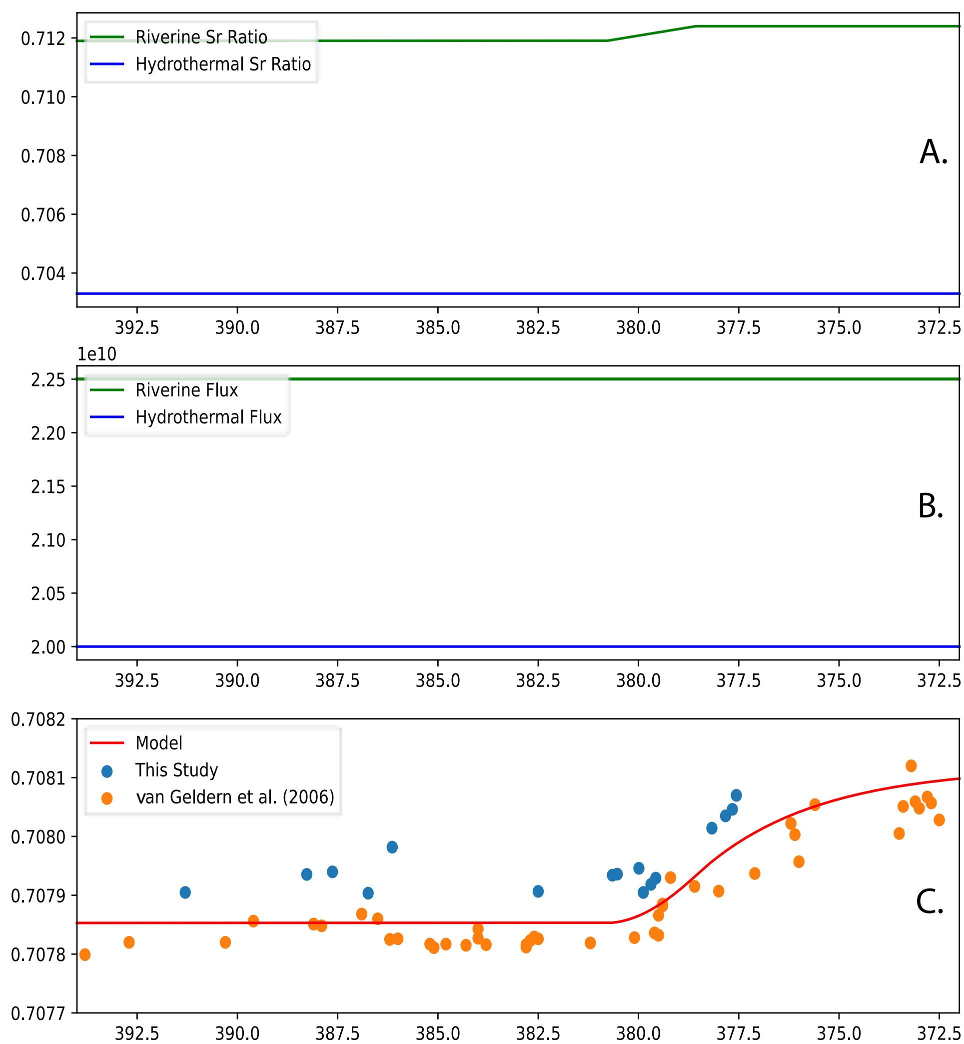

Fig. 5. Sr box model. Panel A shows increase in riverine $^{87}Sr/^{86}Sr$ and a constant hydrothermal $^{87}Sr/^{86}Sr$ ratio. Panel B shows constant riverine and hydrothermal fluxes. See Table S4 for list of initial parameters and text for discussion. Panel C shows the late Givetian increase in $^{87}Sr/^{86}Sr$ based on the model run driven by increasing riverine $^{87}Sr/^{86}Sr$. In Panel C the blue filled circles are data from this study and orange filled circles are from van Geldern et al. (2006). Note that in Panel C the magnitude of the offset between brachiopod calcite (van Geldern et al., 2006) and conodont apatite (this study) maintains a similar range that averages ~0.00011 ± 0.00003. (For interpretation of the references to colour in this figure legend, the reader is referred to the web version of this article.)

We use the Spatial Continuous Integration (SCION) global climate-biogeochemical model (Mills et al., 2021, 2025), which can assign the Acadian land surface a higher $^{87}Sr/^{86}Sr$ than surrounding lithologies (Fig. S4 in Supplementary Material). The model produces pCO_2, surface air temperature (SAT), $\delta^{18}O$, and $^{87}Sr/^{86}Sr$ curves using the timing and magnitude of degassed CO_2 during the Acadian Orogeny (Fig. 6), as predicted by Stewart and Ague (2018). Similar to the COPSE model in Chen et al. (2021), the model produces surface water equatorial warming of <2 °C that is much smaller than the 8 to 10 °C shift predicted by the conodont apatite-based $\delta^{18}O$ curve (Fig. 6B, C). However, the model produces the inflection point to rising $^{87}Sr/^{86}Sr$ values coincident with peak warming after 380 Ma (Fig. 6D).

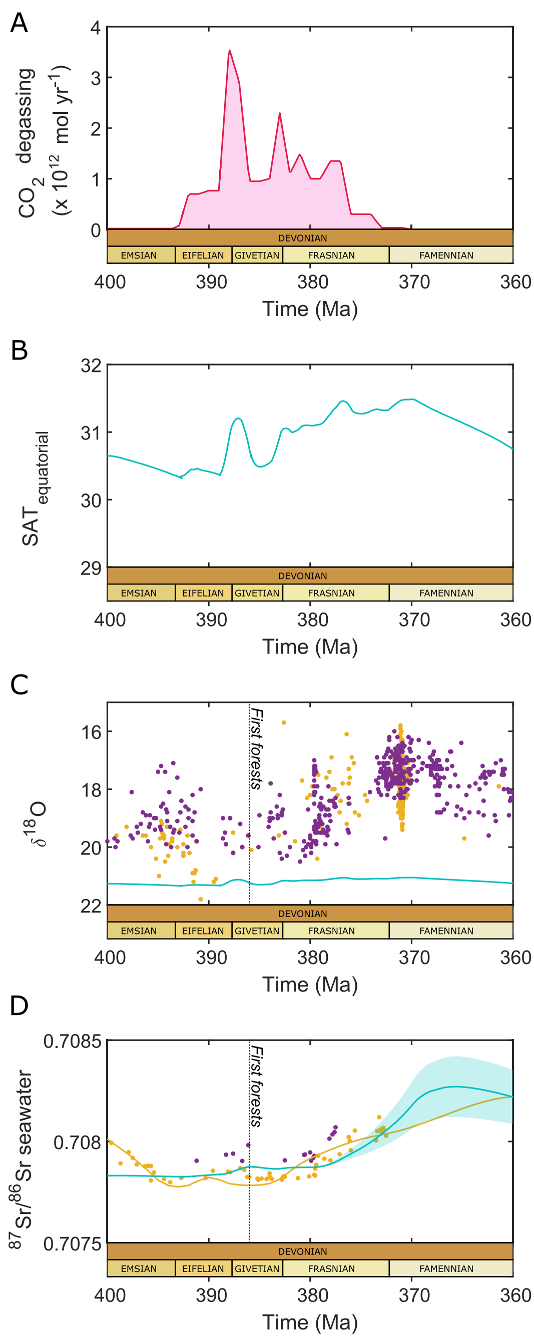

Fig. 6. A. Predicted rate of CO_2 degassing based on Stewart and Ague (2018). B. Surface Air Temperature in degrees C ($SAT_{equatorial}$) calculated from degassing rate shown in panel A. C. Blue curve shows modeled $\delta^{18}O$ based on sea surface temperatures calculated from pCO_2 curve in panel B. $\delta^{18}O$ data from Joachimski et al. (2009) (yellow) and Chen et al. (2021) (purple). D. Modeled $^{87}Sr/^{86}Sr$ (blue line) using SCION. $^{87}Sr/^{86}Sr$ data from this study (purple), van Geldern et al. (2006) (yellow), and McArthur et al. (2020) LOESS curve (yellow). First forests (dotted line) from Chen et al. (2021) and Maffre et al. (2022). (For interpretation of the references to colour in this figure legend, the reader is referred to the web version of this article.)

Whereas SCION can produce a model fit to the $^{87}Sr/^{86}Sr$ curve it does not explain the magnitude of warming observed in the Middle to Late Devonian $\delta^{18}O$ curve. Alternative hypotheses to metamorphic degassing are necessary to explain higher atmospheric CO_2 levels and additional warming, and one possibility is a reduction in silicate weathering efficiency driven by vascular plant colonization as proposed by Maffre et al. (2022). Although land plants have also been considered a driver of enhanced silicate weathering and cooling (e.g., Le Hir et al., 2011), Maffre et al. (2022) instead propose that vascular plants cover exposed silicate rock area and reduce physical erosion, which in turn can lower rates of silicate weathering and raise pCO_2. Maffre et al. (2022) place the first appearance of forests in the early Givetian (Fig. 6) and model a series of scenarios in which pCO_2 rises or oscillates during the Givetian to Frasnian before eventually decreasing from the Frasnian into the Famennian.

Although incorporating the Maffre et al. (2022) scenarios into SCION is beyond the scope of this paper, their hypothesis of reduced silicate weathering with increased plant coverage has implications for our Middle-Late Devonian $^{87}Sr/^{86}Sr$ interpretation. An increase in the riverine flux of Sr or the $^{87}Sr/^{86}Sr$ ratio are plausible scenarios for the $^{87}Sr/^{86}Sr$ rise in the late Givetian. The hypothesis of Maffre et al. (2022) would predict an overall decrease in $^{87}Sr/^{86}Sr$ linked to continental weathering based on plant colonization. In order to counteract the effect of land plant colonization, it is necessary to have a radiogenic (high $^{87}Sr/^{86}Sr$) source rock in upland regions such as the Acadian Orogen (Golonka, 2020; Maffre et al., 2022). Links between $^{87}Sr/^{86}Sr$ as a weathering proxy and $\delta^{18}O$ as a paleotemperature proxy linked to changes in CO_2 at other times in Earth history present similar challenges because a unique interpretation is not possible and other proxies must ultimately be brought to bear on the problem (e.g., Berner and Kothavala, 2001; McKenzie et al., 2016; Macdonald et al., 2019; Liu et al., 2025). For example, a rise in pCO_2 during the Jurassic (Toarcian) potentially driven by volcanism (e.g., Reolid et al., 2021) may relate to enhanced weathering based on increased $^{87}Sr/^{86}Sr$ (Jones et al., 1994) and $^{187}Os/^{186}Os$ (Them et al., 2017). The Middle to Late Ordovician decrease in seawater $^{87}Sr/^{86}Sr$ has been linked to changes in Nd isotopes that signal weathering of uplifted ophiolites in the Taconic Orogeny that coincides with cooling (e.g., Swanson-Hysell and Macdonald, 2017; Conwell et al., 2022; Adiatma et al., 2024).

6. Conclusions

New $^{87}Sr/^{86}Sr$ paired with existing $\delta^{18}O$ data from the same sample set demonstrate a correlation between warming and an increase in the weathering of higher $^{87}Sr/^{86}Sr$ bedrock during the late Givetian. A Sr box model suggests that an ~3% increase in exposed land ±10° of the equator likely contributed to the increase in seawater $^{87}Sr/^{86}Sr$. However, a second box model demonstrates that an increase in the $^{87}Sr/^{86}Sr$ of the riverine weathering flux of Sr starting at around 380 Ma and spanning ~2–3 My is needed to create the observed increase in Sr isotopes. We propose that this theoretical $^{87}Sr/^{86}Sr$ increase was mainly derived from weathering of the Acadian Orogen, which had a granitic (radiogenic) composition.

On a wider scale, the warming of the Middle to Late Devonian marks a departure from the large-scale cooling observed from the Early Devonian into the Carboniferous. This may have been related to the early colonization of the continents by vascular plants, which reduced physical weathering and led to a transient increase in pCO_2. Acadian metamorphic degassing also likely contributed to warming. However, both the previous COPSE model and present SCION model demonstrate that the amount of CO_2 released via decarbonation would have been insufficient to cause equatorial warming of 8 to 10 °C.

CRediT authorship contribution statement

Teresa D. Avila: Methodology, Investigation, Funding acquisition, Formal analysis, Data curation, Conceptualization. **Matthew R. Saltzman:** Writing – review & editing, Methodology, Investigation, Funding acquisition, Conceptualization. **Michael M. Joachimski:** Writing – review & editing, Resources, Formal analysis. **Elizabeth M. Griffith:** Writing – review & editing, Validation, Methodology, Investigation, Formal analysis. **Benjamin J.W. Mills:** Writing – review & editing, Visualization, Software, Methodology, Formal analysis.

Declaration of competing interest

The authors declare that they have no known competing financial interests or personal relationships that could have appeared to influence the work reported in this paper.

Acknowledgments

This work was financially supported by the Friends of Orton Hall from The Ohio State University as well as a Geological Society of America Graduate Student Research Grant.

We thank two anonymous reviewers for their constructive comments and suggestions to improve the manuscript. We thank Anthony Lutton for his assistance in laboratory research. We thank Christopher Conwell and Datu Adiatma for their discussion and input about the ideas presented in this paper.

Appendix A. Supplementary data

Supplementary data to this article can be found online at https://doi.org/10.1016/j.palaeo.2026.114032.

Data availability

The authors confirm that all data necessary for supporting the scientific findings of this paper have been provided.

References

Adiatma, Y.D., Saltzman, M.R., Liu, X.-M., Wang, X.-K., Edwards, C.T., 2024. Lithium isotope stratigraphy and Ordovician weathering. Earth Planet. Sci. Lett. 647, 119030. https://doi.org/10.1016/j.epsl.2024.119030.

Antonelli, M.A., Pester, N.J., Brown, S.T., DePaolo, D.J., 2017. Effect of paleoseawater composition on hydrothermal exchange in midocean ridges. Proc. Natl. Acad. Sci. USA 114, 12413–12418. https://doi.org/10.1073/pnas.1709145114.

Avila, T.D., Saltzman, M.R., Adiatma, Y.D., Joachimski, M.M., Griffith, E.M., Olesik, J. W., 2022. Role of seafloor production versus continental basalt weathering in Middle to late Ordovician seawater 87Sr/86Sr and climate. Earth Planet. Sci. Lett. 593, 117641. https://doi.org/10.1016/j.epsl.2022.117641.

Avila, T.D., Saltzman, M.R., Griffith, E.M., Joachimski, M.M., 2025. Silicate weathering, land plants and cooling in the late Silurian and early Devonian. J. Geol. Soc. 182. https://doi.org/10.1144/jgs2023-148 jgs2023–148.

Bambach, R.K., 2006. Phanerozoic Biodiversity Mass Extinctions. Annu. Rev. Earth Planet. Sci. 34, 127–155. https://doi.org/10.1146/annurev.earth.33.092203.122654.

Basu, A.R., Jacobsen, S.B., Poreda, R.J., Dowling, C.B., Aggarwal, P.K., 2001. Large Groundwater Strontium Flux to the Oceans from the Bengal Basin and the Marine Strontium Isotope Record. Science 293, 1470–1473. https://doi.org/10.1126/science.1060524.

Becker, R.T., Marshall, J.E.A., Da Silva, A.-C., Agterberg, F.P., Gradstein, F.M., Ogg, J.G., 2020. The Devonian Period. In: Geologic Time Scale 2020. Elsevier, pp. 733–810.

Berner, R.A., Kothavala, Z., 2001. GEOCARB III: a revised model of atmospheric CO2 over Phanerozoic time. Am. J. Sci. 301, 182–204. https://doi.org/10.2475/ajs.301.2.182.

Buggisch, W., Joachimski, M.M., 2006. Carbon isotope stratigraphy of the Devonian of Central and Southern Europe. Palaeogeogr. Palaeoclimatol. Palaeoecol. 240, 68–88. https://doi.org/10.1016/j.palaeo.2006.03.046.

Chen, B., Ma, X., Mills, B.J.W., Qie, W., Joachimski, M.M., Shen, S., Wang, C., Xu, H., Wang, X., 2021. Devonian paleoclimate and its drivers: a reassessment based on a new conodont δ18O record from South China. Earth Sci. Rev. 222, 103814. https://doi.org/10.1016/j.earscirev.2021.103814.

Chenery, C., Müldner, G., Evans, J., Eckardt, H., Lewis, M., 2010. Strontium and stable isotope evidence for diet and mobility in Roman Gloucester, UK. J. Archaeol. Sci. 37, 150–163. https://doi.org/10.1016/j.jas.2009.09.025.

Conwell, C.T., Saltzman, M.R., Edwards, C.T., Griffith, E.M., Adiatma, Y.D., 2022. Nd isotopic evidence for enhanced mafic weathering leading to Ordovician cooling. Geology 50, 886–890. https://doi.org/10.1130/G49860.1.

Conwell, C.T., Saltzman, M.R., Lindskog, A., Eriksson, M.E., Griffith, E.M., Leslie, S.A., Edwards, C.T., Hints, O., Herrmann, A.D., 2026. Factors affecting 87Sr/86Sr preservation in conodont apatite: an example from the Ordovician of Baltoscandia. Palaeogeogr. Palaeoclimatol. Palaeoecol. 685, 113524. https://doi.org/10.1016/j.palaeo.2025.113524.

Coogan, L.A., Gillis, K.M., 2018. Low-Temperature Alteration of the Seafloor: Impacts on Ocean Chemistry. Annu. Rev. Earth Planet. Sci. 46, 21–45. https://doi.org/10.1146/annurev-earth-082517-010027.

Dahl, T.W., Arens, S.K.M., 2020. The impacts of land plant evolution on Earth's climate and oxygenation state – an interdisciplinary review. Chem. Geol., 119665 https://doi.org/10.1016/j.chemgeo.2020.119665.

Denison, R.E., Koepnick, R.B., Burke, W.H., Hetherington, E.A., Fletcher, A., 1997. Construction of the Silurian and Devonian seawater 87Sr86Sr curve. Chem. Geol. 140, 109–121.

Dudás, F., Yuan, D.X., Shen, S.Z., Bowring, S.A., 2017. A conodont-based revision of the 87Sr/86Sr seawater curve across the Permian-Triassic boundary. Palaeogeogr. Palaeoclimatol. Palaeoecol. 470, 40–53. https://doi.org/10.1016/j.palaeo.2017.01.007.

Elderfield, H., Schultz, A., 1996. Mid-Ocean Ridge Hydrothermal Fluxes and the Chemical Composition of the Ocean. Annu. Rev. Earth Planet. Sci. 24, 191–224. https://doi.org/10.1146/annurev.earth.24.1.191.

Elrick, M., 2022. Orbital-scale climate changes detected in lower and Middle Ordovician cyclic limestones using oxygen isotopes of conodont apatite. Palaeogeogr. Palaeoclimatol. Palaeoecol. 603, 111209. https://doi.org/10.1016/j.palaeo.2022.111209.

Elrick, M., Berkyová, S., Klapper, G., Sharp, Z., Joachimski, M., Frýda, J., 2009. Stratigraphic and oxygen isotope evidence for My-scale glaciation driving eustasy in the Early–Middle Devonian greenhouse world. Palaeogeogr. Palaeoclimatol. Palaeoecol. 276, 170–181. https://doi.org/10.1016/j.palaeo.2009.03.008.

Elrick, M., Gilleaudeau, G.J., Romaniello, S.J., Algeo, T.J., Morford, J.L., Sabbatino, M., Goepfert, T.J., Cleal, C., Cascales-Miñana, B., Chernyavskiy, P., 2022. Major Early-Middle Devonian oceanic oxygenation linked to early land plant evolution detected using high-resolution U isotopes of marine limestones. Earth Planet. Sci. Lett. 581, 117410. https://doi.org/10.1016/j.epsl.2022.117410.

Emsbo, P., Premo, W.R., McLaughlin, P.I., Neymark, L.A., Vandenbroucke, T.R.A., Day, J. (Jed) E., Bray, E.A.D., Manning, A.H., Bancroft, A.M., 2018. Impact of Sedimentary-Exhalative Hydrothermal Systems on Marine Chemistry and Mass Extinctions: Applications for Ore Genesis Research and Mineral Exploration. In: Arribas R., A.M., Mauk, J.L. (Eds.), Metals, Minerals, and Society. Society of Economic Geologists, pp. 75–87. https://doi.org/10.5382/SP.21.05.

Epstein, A.G., Epstein, J.B., Harris, L.D., 1977. Conodont Color Alteration- an Index to Organic Metamorphism. United States Geological Survey, Washington D.C.

Feist, R., 1985. Devonian stratigraphy of the south-eastern Montagne Noir (France). CFS Cour. Forschungsinstitut Senckenberg 75, 331–352.

Feist, R., 2002. International Union of Geological Sciences, IGCP 421: North Gondwana Mid-Palaeozoic Biodynamics and ECOS VIII: 8th European Conodont Symposium. The Palaeozoic of the Montagne Noire, Southern France.

Foland, K.A., Allen, J.C., 1991. Magma sources for Mesozoic anorogenic granites of the White Mountain magma series, New England, USA. Contrib. Mineral. Petrol. 109, 195–211.

Gaffin, S., 1987. Ridge volume dependence on seafloor generation rate and inversion using long term sealevel change. Am. J. Sci. 287, 596–611.

van Geldern, R., Joachimski, M.M., Day, J., Jansen, U., Alvarez, F., Yolkin, E.A., Ma, X.-P., 2006. Carbon, oxygen and strontium isotope records of Devonian brachiopod shell calcite. Palaeogeogr. Palaeoclimatol. Palaeoecol. 240, 47–67. https://doi.org/10.1016/j.palaeo.2006.03.045.

Golonka, J., 2020. Late Devonian paleogeography in the framework of global plate tectonics. Glob. Planet. Chang. 186. https://doi.org/10.1016/j.gloplacha.2020.103129.

Grossman, E.L., Joachimski, M.M., 2022. Ocean temperatures through the Phanerozoic reassessed. Sci. Rep. 12, 8938. https://doi.org/10.1038/s41598-022-11493-1.

Haq, B.U., Schutter, S.R., 2008. A chronology of paleozoic sea-level changes. Science 322, 64–68. https://doi.org/10.1126/science.1161648.

Holmden, C., 1996. Isotopic and elemental systematics of Sr and Nd in 454 Ma biogenic apatites: implications for paleoseawater studies. Earth Planet. Sci. Lett. 142, 425–437. https://doi.org/10.1016/0012-821X(96)00119-7.

Huang, J., Kershaw, S., Liang, K., Qie, W., 2025. The South China Block: a reef-building focal point in Givetian (Middle Devonian) of eastern Palaeotethys. Earth Sci. Rev. 269, 105202. https://doi.org/10.1016/j.earscirev.2025.105202.

Ingram, B.L., Coccioni, R., Montanari, A., Richter, F.M., 1994. Strontium Isotopic Composition of Mid-cretaceous Seawater. Science 264, 546–550. https://doi.org/10.1126/science.264.5158.546.

Joachimski, M.M., Breisig, S., Buggisch, W., Talent, J.A., Mawson, R., Gereke, M., Morrow, J.R., Day, J. (Jed) E., Weddige, K., 2009. Devonian climate and reef evolution: insights from oxygen isotopes in apatite. Earth Planet. Sci. Lett. 284, 599–609. https://doi.org/10.1016/j.epsl.2009.05.028.

John, E.H., Cliff, R., Wignall, P.B., 2008. A positive trend in seawater $^{87}Sr/^{86}Sr$ values over the Early–Middle Frasnian boundary (Late Devonian) recorded in well-

preserved conodont elements from the Holy Cross Mountains, Poland. Palaeogeogr. Palaeoclimatol. Palaeoecol. 269, 166–175. https://doi.org/10.1016/j.palaeo.2008.04.031.
Jones, C.E., Jenkyns, H.C., 2001. Seawater strontium isotopes, oceanic anoxic events, and seafloor hydrothermal activity in the Jurassic and cretaceous. Am. J. Sci. 301, 112–149. https://doi.org/10.2475/ajs.301.2.112.
Jones, C.E., Jenkyns, H.C., Coe, A.L., Stephen, H.P., 1994. Strontium isotopic variations in Jurassic and cretaceous seawater. Geochim. Cosmochim. Acta 58, 3061–3074. https://doi.org/10.1016/0016-7037(94)90179-1.
Kabanov, P., Hauck, T.E., Gouwy, S.A., Grasby, S.E., Van Der Boon, A., 2023. Oceanic anoxic events, photic-zone euxinia, and controversy of sea-level fluctuations during the Middle-late Devonian. Earth Sci. Rev. 241, 104415. https://doi.org/10.1016/j.earscirev.2023.104415.
Le Hir, G., Donnadieu, Y., Goddéris, Y., Meyer-Berthaud, B., Ramstein, G., Blakey, R.C., 2011. The climate change caused by the land plant invasion in the Devonian. Earth Planet. Sci. Lett. 310, 203–212. https://doi.org/10.1016/j.epsl.2011.08.042.
Lenton, T.M., Daines, S.J., Mills, B.J.W., 2018. COPSE reloaded: an improved model of biogeochemical cycling over Phanerozoic time. Earth Sci. Rev. 178, 1–28. https://doi.org/10.1016/j.earscirev.2017.12.004.
Liu, X., Krause, A.J., Wilson, D.J., Fraser, W.T., Joachimski, M.M., Brand, U., Stigall, A.L., Qie, W., Chen, B., Yang, X., Pogge Von Strandmann, P.A.E., 2025. Lithium isotope evidence shows Devonian afforestation may have significantly altered the global silicate weathering regime. Geochim. Cosmochim. Acta 396, 107–121. https://doi.org/10.1016/j.gca.2025.02.036.
Macdonald, F.A., Swanson-Hysell, N.L., Park, Y., Lisiecki, L., Jagoutz, O., 2019. Arc-continent collisions in the tropics set Earth's climate state. Science 364, 181–184. https://doi.org/10.1126/science.aav5300.
Maffre, P., Godderis, Y., Pohl, A., Donnadieu, Y., Carretier, S., Le Hir, G., 2022. The complex response of continental silicate rock weathering to the colonization of the continents by vascular plants in the Devonian. Am. J. Sci. 322, 461–492. https://doi.org/10.2475/03.2022.02.
Marcilly, C.M., Torsvik, T.H., Domeier, M., Royer, D.L., 2021. New paleogeographic and degassing parameters for long-term carbon cycle models. Gondwana Res. 97, 176–203. https://doi.org/10.1016/j.gr.2021.05.016.
Martin, E.E., Scher, H.D., 2004. Preservation of seawater Sr and Nd isotopes in fossil fish teeth: bad news and good news. Earth Planet. Sci. Lett. 220, 25–39. https://doi.org/10.1016/S0012-821X(04)00030-5.
McArthur, J.M., Howarth, R.J., Shields, G.A., Zhou, Y., 2020. Strontium Isotope Stratigraphy. In: Geologic Time Scale 2020. Elsevier, pp. 211–238. https://doi.org/10.1016/B978-0-12-824360-2.00007-3.
McKenzie, R.N., Horton, B.K., Loomis, S.M., Stockli, D.F., Planavsky, N.J., Lee, C.-T.A., 2016. Continental arc volcanism as the principal driver of icehouse-greenhouse variability. Science 352, 444–447. https://doi.org/10.1126/science.aad5787.
Mills, B.J.W., Scotese, C.R., Walding, N.G., Shields, G.A., Lenton, T.M., 2017. Elevated CO2 degassing rates prevented the return of Snowball Earth during the Phanerozoic. Nat. Commun. 8, 1–7. https://doi.org/10.1038/s41467-017-01456-w.
Mills, B.J.W., Donnadieu, Y., Goddéris, Y., 2021. Spatial continuous integration of Phanerozoic global biogeochemistry and climate. Gondwana Res. 100, 73–86. https://doi.org/10.1016/j.gr.2021.02.011.
Mills, B.J.W., Le Hir, G., Merdith, A., Gurung, K., Bowyer, F.T., Krause, A.J., Sanchez-Baracaldo, P., Hunter, S.J., Zhang, Y., 2025. Exploring Neoproterozoic climate and biogeochemical evolution in the SCION model. Glob. Planet. Chang. 249, 104791. https://doi.org/10.1016/j.gloplacha.2025.104791.
Murphy, J.B., Keppie, J.D., 2005. The acadian orogeny in the northern appalachians. Int. Geol. Rev. 47, 663–687. https://doi.org/10.2747/0020-6814.47.7.663.
Peucker-Ehrenbrink, B., Fiske, G.J., 2019. A continental perspective of the seawater 87Sr/86Sr record: a review. Chem. Geol. 510, 140–165. https://doi.org/10.1016/j.chemgeo.2019.01.017.
Qie, W.-K., Algeo, T.J., Luo, G., Herrmann, A.D., 2019. Global events of the late Paleozoic (early Devonian to Middle Permian): a review. Palaeogeogr. Palaeoclimatol. Palaeoecol. 531, 109259. https://doi.org/10.1016/j.palaeo.2019.109259.
Racki, G., 2020. A volcanic scenario for the Frasnian–Famennian major biotic crisis and other Late Devonian global changes: more answers than questions? Glob. Planet. Chang. 189, 103174. https://doi.org/10.1016/j.gloplacha.2020.103174.
Read, J.F., Pope, M.C., Elrick, M., Hinnov, L., Repetski, J., Ryder, R.T., Patchen, D.G., Diecchio, R., 2023. Depositional and tectonic influences on preservation of Milankovitch record during long-term global cooling: Middle and Upper Ordovician convergent foreland, eastern USA. Palaeogeogr. Palaeoclimatol. Palaeoecol. 627, 111738. https://doi.org/10.1016/j.palaeo.2023.111738.
Reolid, M., Mattioli, E., Duarte, L.V., Ruebsam, W., 2021. The Toarcian Oceanic Anoxic Event: where do we stand? Geol. Soc. Lond. Spec. Publ. 514, 1–11. https://doi.org/10.1144/SP514-2021-74.
Saltzman, M.R., Edwards, C.T., Leslie, S.A., Dwyer, G.S., Bauer, J.A., Repetski, J.E., Harris, A.G., Bergström, S.M., 2014. Calibration of a conodont apatite-based Ordovician 87Sr/86Sr curve to biostratigraphy and geochronology: Implications for stratigraphic resolution. Bull. Geol. Soc. Am. 126, 1551–1568. https://doi.org/10.1130/B31038.1.
Scher, H.D., Griffith, E.M., Buckley, W.P., 2014. Accuracy and precision of 88Sr/86Sr and 87Sr/86Sr measurements by MC-ICPMS compromised by high barium concentrations. Geochem. Geophys. Geosyst. 15, 499–508. https://doi.org/10.1002/2013GC005134.
van Staal, C.R., Whalen, J.B., Valverde-Vaquero, P., Zagorevski, A., Rogers, N., 2009. Pre-Carboniferous, episodic accretion-related, orogenesis along the Laurentian margin of the northern Appalachians. In: Murphy, J.B., Keppie, J.D., Hynes, a.J. (Eds.), Ancient Orogens and Modern Analogues, 327. Geological Society, London, Special Publications, pp. 271–316. https://doi.org/10.1144/SP327.13.
Steiger, R.H., Jäger, E., 1977. Subcomission on Geochronology: Convention on the use of decay constants in geo- and cosmochronology. Earth Planet. Sci. Lett. 36, 359–362.
Stewart, E.M., Ague, J.J., 2018. Infiltration-driven metamorphism, New England, USA: Regional CO2 fluxes and implications for Devonian climate and extinctions. Earth Planet. Sci. Lett. 489, 123–134. https://doi.org/10.1016/j.epsl.2018.02.028.
Swanson-Hysell, N.L., Macdonald, F.A., 2017. Tropical weathering of the Taconic orogeny as a driver for Ordovician cooling. Geology 45, 719–722. https://doi.org/10.1130/G38985.1.
Them, T.R., Gill, B.C., Selby, D., Gröcke, D.R., Friedman, R.M., Owens, J.D., 2017. Evidence for rapid weathering response to climatic warming during the Toarcian Oceanic Anoxic Event. Sci. Rep. 7, 5003. https://doi.org/10.1038/s41598-017-05307-y.
Torsvik, T.H., Cocks, L.R.M., 2017. Earth History and Palaeogeography. Cambridge University Press, Cambridge, United Kingdom.
Zhang, L., Algeo, T.J., Zhao, H., Lyu, Z., Hao, F., 2026. Diagenetic effects on conodont oxygen-isotopic compositions: implications for in-situ analysis and paleothermometry. Geochim. Cosmochim. Acta 421, 455–473. https://doi.org/10.1016/j.gca.2026.02.031.